NMR in Biomedicine

WILEY

NMR IN BIOMEDICINE

RESEARCH ARTICLE OPEN ACCESS

Capturing Acute and Subchronic Myocardial Infarct by MRI Rotating Frame Relaxation Times in Mice In and Ex Vivo

Elias Ylä-Herttuala[1,2] | Hanne Laakso[1] | Muhammad Arsalan Khan[1] | Svetlana Laidinen[1] | Tommi Heikura[1] | Seppo Ylä-Herttuala[1,3] | Timo Liimatainen[4,5]

[1]Department of Biotechnology and Molecular Medicine, A.I. Virtanen Institute for Molecular Sciences, University of Eastern Finland, Kuopio, Finland | [2]Clinical Radiology Unit, Imaging Center, Kuopio University Hospital, Kuopio, Finland | [3]Heart Center, Kuopio University Hospital, Kuopio, Finland | [4]Research Unit for Medical Imaging, Physics and Technology, University of Oulu, Oulu, Finland | [5]Department of Diagnostic Radiology, Oulu University Hospital, Oulu, Finland

Correspondence: Elias Ylä-Herttuala (elias.yla-herttuala@uef.fi)

Received: 6 February 2025 | **Revised:** 13 April 2025 | **Accepted:** 28 April 2025

Funding: The authors thank the following funding agency for providing funding to be used as a personal grant: Sigrid Juselius Foundation, Finnish Foundation for Cardiovascular Research, Finnish Cultural Foundation, Emil Aaltonen Foundation, State Research Funding, and GeneCellNano Flagship Program.

Keywords: CMRI | MI | rotating frame methods | $T_{1\rho}$ | $T_{2\rho}$

ABSTRACT

Cardiovascular diseases are the leading cause of death worldwide due to population growth and aging. Myocardial infarct is one of the most crucial cardiovascular diseases. Acute myocardial infarct is conventionally imaged with magnetic resonance imaging (MRI) with T_2 mapping due to its sensitivity related to the correlation times of edema and free water molecules. Chronic myocardial infarction, which contains fibrosis and scar tissue, is conventionally imaged with MRI by using contrast agents since contrast agent washout from fibrosis and scar tissue is delayed compared to myocardium. Rotating frame relaxation times $T_{1\rho}$ and $T_{2\rho}$ mappings were developed to provide robust measurements with relatively wide B_1 and B_0 ranges for these quantities. Since rotating frame methods are sensitive to slow molecular motions, these methods owe potential to characterize both acute and chronic myocardial infarctions. In this study, rotating frame relaxation time mappings were applied to image acute (2 h) and subchronic (7 days after occlusion) myocardial infarcts in in vivo and ex vivo mouse models without using contrast agents. The in vivo imaging protocol contained adiabatic $T_{1\rho}$ and adiabatic $T_{2\rho}$, both with hyperbolic secant (HS) 1 and 4 pulses, continuous wave $T_{1\rho}$ and conventional T_2, together with cine imaging. Mice were imaged 2 h and 7 days after myocardial infarction. Mice were sacrificed at the 2-h or 7-day time point. Ex vivo measurements contained adiabatic $T_{1\rho}$ and adiabatic $T_{2\rho}$ with HS1 and HS4 pulses, continuous wave $T_{1\rho}$, T_1, and T_2. After MRI studies, mouse hearts were fixed, and myocardial infarcts were verified using dystrophin and hematoxylin and eosin histology stainings. A clear difference between infarcted and normal myocardium was visible at the 2-h time point in rotating frame relaxation time mapping. Relative relaxation time difference in adiabatic $T_{2\rho}$ with HS4 pulse showed the significant differences between MI and control hearts in vivo. In addition, the results of adiabatic $T_{1\rho}$ with both HS1 and HS4 pulses and continuous wave $T_{1\rho}$ measurements showed significant differences between MI and control hearts

Abbreviations: B_{eff}, effective radio frequency field; CW, continuous wave; HS, hyperbolic secant; LAD, left anterior descending (artery); LGE, late gadolinium enhancement; M, magnetization; MI, myocardial infarction; PBS, phosphate buffered saline; PFA, paraformaldehyde; ROI, region of interest; RRTD, relative relaxation time difference; $T_{1\rho}$, longitudinal rotating frame relaxation time; $T_{2\rho}$, transversal rotating frame relaxation time.

Hanne Laakso and Muhammad Arsalan Khan share equal contribution.

at both time points in both in vivo and ex vivo measurements. This study shows that rotating frame relaxation time mappings have the potential to be noninvasive MR diagnostic markers for acute and subchronic myocardial infarcts.

1 | Introduction

Cardiovascular diseases (CVDs) are the leading cause of death worldwide due to population growth and an aging population [1], myocardial infarction (MI) being one of the most crucial CVDs. MI occurs when the coronary artery is either fully or partly occluded, causing a disturbance to the perfusion [2]. Occlusion can lead to a hibernating infarct or complete infarct when the myocardium lacks oxygen, leading to necrotic cell loss and finally to scar formation or, in the worst case, heart failure [3].

Cardiac magnetic resonance imaging (MRI) provides an accurate assessment of the anatomy and the function of the myocardium [4]. Functional cardiac MRI is usually done by gradient echo-based cine MRI, where volumetric parameters of the short-axis view of the left ventricle can be calculated [4]. Late gadolinium enhancement (LGE) is the gold standard to assess MI [4]. LGE images are acquired so that the area of MI has a hyperintense signal as compared to remote myocardium in the gray-scale image of myocardium [4, 5]. This is due to the delayed clearance of gadolinium (Gd) from the MI tissue [4, 5]. Increased late Gd accumulation in the MI area has been associated with increased extracellular space [6]. LGE is a qualitative method to determine the MI area; however, LGE has a few drawbacks, including that it shows only expanded extracellular matrix; thus, it is not specific, has challenges in diffuse fibrosis detection, and has limitations in its use for patients with renal injury and for pregnant women [6].

The heart and the MI area can also be imaged with conventional endogenous MRI contrasts, such as T_1- and T_2-weighted MRI techniques. The T_1 relaxation time constant has been shown to increase in the MI compared to a remote area [4]. The T_2 relaxation time constant has been used to quantify myocardial edema caused by either inflammation or ischemic insult, and therefore, the T_2 relaxation time constant has been used to determine the edema in acute MI. While conventional T_1 and T_2 relaxations occur during free precession after the radio frequency (RF) excitation pulse, rotating frame relaxations occur during RF excitation [7, 8]. The spin-lock field is a vector sum of the RF pulse magnetic field component (B_1) perpendicular to the main magnetic field (B_0) and the off-resonance component along B_0 [6, 9]. Relaxation in the rotating frame occurs either along ($T_{1\rho}$) or transversal ($T_{2\rho}$) to the effective magnetic field (B_{eff}) that acts as a spin-lock field. The amplitudes of B_{eff} and RF pulses are typically between 0.1 and 10 kHz, making rotating frame relaxations sensitive to slow molecular fluctuations close to the corresponding frequency ranges [6, 9]. Proton chemical exchange between free water ^1H and ^1H of the exchanging groups of other molecules, usually macromolecules, is typically in the same frequency range [6, 9].

$T_{1\rho}$ rotating frame relaxation time constants can be performed with a continuous wave (CW) RF pulse or adiabatic RF pulses. In the CW $T_{1\rho}$, a composite RF pulse consisting of a 90° hard pulse [10, 11] or an adiabatic half passage (AHP) [12] pulse is followed by a CW pulse to lock the spins and finally a 90° hard pulse or reverse AHP to return the magnetization (M) back to the B_0 direction (Figure 1). After the composite weighting pulse, the signal can be acquired with a readout sequence. MI area has been determined with CW $T_{1\rho}$ at multiple time points in mice [9, 13, 14], in swine [10], and in humans [15]. A common factor in these studies has been that a significant increase in the $T_{1\rho}$ relaxation time constant in the MI area compared to remote myocardium has been found with a clear contrast between the MI and remote areas in the CW $T_{1\rho}$ relaxation time maps [9, 10, 13, 14].

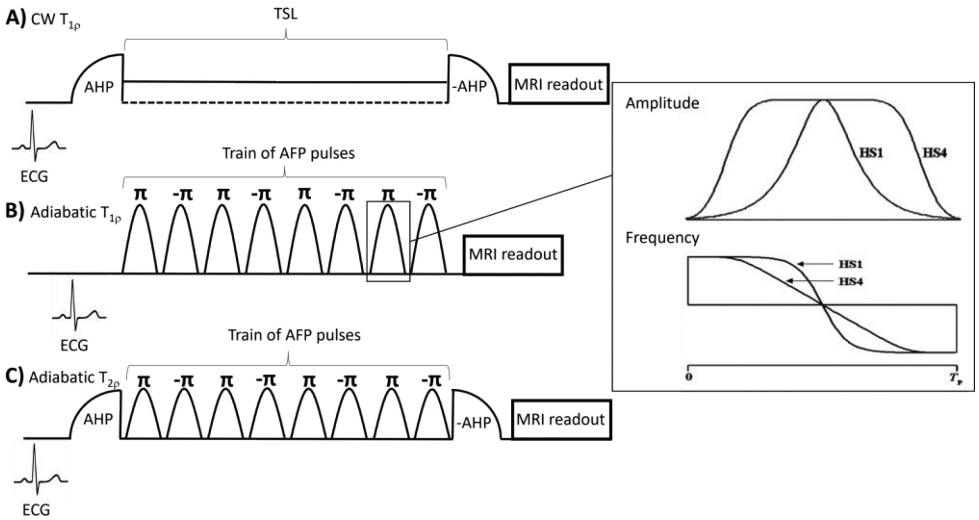

FIGURE 1 | A schematic view of rotating frame magnetization preparations applied between the ECG trigger and readout sequence. (A) Continuous wave (CW) $T_{1\rho}$, (B) adiabatic $T_{1\rho}$, and (C) adiabatic $T_{2\rho}$. In adiabatic $T_{1\rho}$ and $T_{2\rho}$ pulse sequences, a train of adiabatic full-passage RF pulses is used. The amplitude and frequency modulations of HS1 and HS4 RF pulses are shown in an insert. AHP, adiabatic half passage; AFP, adiabatic full passage; TSL, spin lock time; Tp, pulse duration.

Additionally, a good agreement between the MI area defined from CW $T_{1\rho}$ relaxation time maps and LGE was found in mice [9], in swine [10], and in humans [15].

Another way to perform the $T_{1\rho}$ rotating frame relaxation time experiments is to use a train of adiabatic RF pulses. The pulses in the train are typically adiabatic full passage (AFP) pulses from the hyperbolic secant (HS) pulse family (Figure 1) [16, 17]. Weighting can be tuned by altering the stretching factor n in adiabatic HSn pulses [16, 17]. Typically, *n* is 1 or 4, leading to HS1 and HS4 pulses, respectively (Figure 1) [16–19]. The difference between the HS1 and HS4 pulses is in the amplitude and frequency modulation functions [16, 17]. HS4 delivers more RF power into tissue than HS1, causing a difference in M decay during the pulse train [16, 17]. When the adiabatic condition [18] is fulfilled, depending on the initial orientation of M according to time-dependent B_{eff} and with respect to the B_0, M decays with $T_{1\rho}$, $T_{2\rho}$, or a combination of them [16, 19, 20]. However, the choice of parameters of the RF pulses, or choices of the amplitude- and frequency-modulation functions, affects the M decay during the pulse train, followed by differences in $T_{1\rho}$ and $T_{2\rho}$ relaxations [17].

$T_{1\rho}$ adiabatic pulses before and after CW pulses were used to measure $T_{1\rho}$ relaxation time constants in ex vivo and in vivo in different ischemic, including MI, and nonischemic CVD patients at 1.5 T [21]. It was found that $T_{1\rho}$ relaxation time constants were increased in the MI area compared to the rest of the myocardium [21]. Adiabatic $T_{1\rho}$ with HS1 pulse trains without CW pulses has been used to characterize 7-day-old mouse MI ex vivo heart [22] and to image healthy volunteers at 3 T to gain information about the behavior of $T_{1\rho}$ adiabatic pulses and to get to know the range of $T_{1\rho}$ relaxation time constants with adiabatic pulses in the normal myocardium [23]. To the best of our knowledge, neither adiabatic $T_{2\rho}$ methods with different lengths of adiabatic HS1 and HS4 pulse trains have been used in the imaging of mouse MI. Additionally, acute MI (2-h time point after MI) is, to our knowledge, rarely used in mouse studies.

In this study, we characterized MI, remote, and intact myocardium in a mouse model by using adiabatic pulse trains for acquiring $T_{1\rho}$ or $T_{2\rho}$ relaxation time methods and for acquiring $T_{1\rho}$ relaxation time method with CW pulses at acute (2 h) and chronic (7 days) time points. The measurements were performed in vivo and ex vivo, and the rotating frame relaxation time maps were visually compared to conventional relaxation time methods, cine images, dystrophin immunostaining, and hematoxylin and eosin (HE)–stained histology sections.

2 | Methods

Fourteen male mice (C57BL/6J, obtained from the Animal Center of the University of Eastern Finland) weighing 20–30 g were divided into two groups: the first group with 10 left anterior descending (LAD) artery-occluded mice and the second group with four control mice with intact hearts. In vivo measurements were successfully performed in 11 mice (seven mice for the 2-h time point, five mice with also the 7-day time point, and four controls). Three mice could not tolerate the imaging anesthesia at 2 h after the LAD operation. Two out of these three mice had MI at a 2-h time point and were included in the ex vivo measurements. Additionally, two mice were sacrificed at the 2-h time point after in vivo MRI for ex vivo measurements. Therefore, the ex vivo measurements were performed in all 14 hearts. All animal experiments were performed according to the national and international guidelines for laboratory animal use and under license ESAVI-270-04.10.07-2017 approved by the National Animal Experiment Board of Finland. All procedures performed in this study were in accordance with the ethical standards of the National Animal Experiment Board in Finland. All the experiments conformed to the Animal Research Reporting In Vivo Experiments (ARRIVE) guidelines.

2.1 | LAD Occlusion

A novel surgical procedure was performed to occlude the LAD artery [9]. Briefly, inhalation anesthesia was induced with 4% isoflurane and maintained with 1.5%–2% isoflurane in a mixture of oxygen and nitrogen, 30%/70%, respectively. The chest was opened at the fourth intercostal space of the sternum in the surgical procedure. The heart was partly pulled out, and the pericardial sac was removed to perform the LAD occlusion. The ligation was performed, the heart was returned to its original position, and the chest was closed between the third and fourth ribs. Analgesia was given on the operation day and the following 2 days: buprenorphine (0.3 mg/mL) (Temgesic 0.05–0.1 mg/kg) and carprofen (5 mg/mL) (Rimadyl 5 mg/kg) for analgesia subcutaneously.

2.2 | Animal Handling in MRI

Mice were anesthetized and kept under inhalation anesthesia during the MRI similarly as described for maintenance during the LAD occlusion operation. A pad circulating warm water maintained the body temperature of the animal close to 37°C. Mice were placed in a prone position with the heart positioned at the magnet's isocenter. Electrocardiography (ECG) was monitored using needle electrodes from forepaws and respiration with a pneumatic pillow using a small animal gating device (Small Animal Instruments Inc., NY, United States). Cardiac and respiratory motion artifacts were minimized by double triggering with ECG and respiration.

2.3 | MRI

MRI data were acquired with a horizontal 9.4 T Varian/Agilent DirectDrive (Agilent Inc., Palo Alto, CA, United States) system with a 31 cm bore size, equipped with a Varian/Agilent DirectDrive console (Agilent Inc., Palo Alto, CA, United States), and with a gradient set bore diameter of 12 cm with a maximum gradient amplitude of 600 m/Tm. A volume quadrature RF transceiver coil of 35 mm diameter (Rapid Biomed GmbH, Rimpar, Germany) was used for the measurements. MR cine images were acquired by ECG-triggered gradient echo sequence (repetition time [TR] = 10 ms and echo time [TE] = 1.3 ms, 10–15 frames per heart cycle, flip angle = 15°, averages = 2,

field-of-view = 30 × 30 mm^2, matrix size = 256 × 256). Cine images were used to select the short-axis slice close to the apex for in vivo relaxation time measurements.

CW $T_{1\rho}$ [24], adiabatic $T_{1\rho}$ [16, 25], T_2, and adiabatic $T_{2\rho}$ [19] were used in this study to image the heart in the diastolic phase of the heart cycle. For in vivo relaxation time measurements, a TurboFLASH gradient echo sequence (TR between the excitations = 3.1 ms, TE = 1.6 ms, flip angle = 25°, data matrix of 128 × 128 with 1 mm slice thickness and averages = 1) was used as a readout sequence. A delay of at least 2 s was applied after each acquisition, followed by respiration triggering. The scanning times for $T_{1\rho}$, T_2, and $T_{2\rho}$ measurements were 4 min each. B_1 field homogeneity was measured to check the data quality. B_1 measurements were also performed using the matrix size = 128 × 64, using a hard pulse with a nominal power of 625 Hz with durations of 0, 0.125, 0.25, 0.375, 0.5, 0.625, 0.75, 0.875, and 1.0 ms. The scan time for B_1 measurements was 1 min.

An illustrative figure of the differences between CW $T_{1\rho}$, adiabatic $T_{1\rho}$, and adiabatic $T_{2\rho}$ is shown in Figure 1. For CW $T_{1\rho}$ measurements, an AHP (duration = 4000 μs and RF power = 1250 Hz) was used to flip M to the *xy*-plane, followed by a CW spin-lock pulse with durations of 0, 18, 36, and 54 ms and RF pulse power = 625 Hz to create a spin-lock field, and an AHP to return the M to the *z*-axis before signal readout. The phases of the AHPs and CW pulse formed a continuous function in the pulse train (Figure 1). In the adiabatic $T_{1\rho}$ and adiabatic $T_{2\rho}$ measurements, the number of HS pulses (durations of 4525 μs, RF power 625 Hz) was 0, 8, 16, 24, and 32 in the pulse train (Figure 1). In $T_{2\rho}$, an AHP pulse (duration = 4000 μs, RF power = 2500 Hz) to tip the M to the *xy*-plane was placed before, and a similar but time-reversed AHP pulse after the AFP pulse train (Figure 1). In both the HS1 and HS4 methods, the spin-lock field was 625 Hz.

All the ex vivo measurements were done at a vertical 9.4 T Varian/Agilent DirectDrive (Agilent Inc., Palo Alto, CA, United States) using a volume RF transceiver coil of diameter 10 mm (Rapid Biomedical GmbH, Rimpar, Germany) and a VnmrJ3.1 Varian/Agilent DirectDrive console. The hearts were placed in an 8-mm NMR glass tube and filled with perfluoropolyether (Galden HS 240, Solvay Solexis, Italy), which is a fluorinated heat transfer fluid that gives no ^{1}H signal in MRI. Ex vivo imaging protocols included T_1, adiabatic $T_{1\rho}$ (with both HS1 and HS4 pulses), adiabatic $T_{2\rho}$ (with both HS1 and HS4 pulses), CW $T_{1\rho}$, and T_2 methods. Adiabatic $T_{1\rho}$, adiabatic $T_{2\rho}$, CW $T_{1\rho}$, and T_2 ex vivo measurements were done using the same parameters as in vivo measurements. T_1 measurements were conducted using inversion recovery with inversion times of 0.01, 0.25, 0.5, 1, and 2 s.

For all the ex vivo measurements, a fast spin echo readout sequence (TR = 2000 ms, effective TE = 9.42 ms, averages = 4 with data matrix = 192 × 128, FOV = 10 mm × 10 mm, resolution 52 μm × 78 μm, echo train length = 4, and slice thickness = 0.70 mm) was used.

2.4 | Histology

After the last imaging time point, the mice were sacrificed with CO_2, and the hearts were collected for histopathology. Eleven animals (10 occluded and one control) were sacrificed after MR measurements for histology. The excised hearts were rinsed with phosphate buffered saline (PBS) and fixed with 4% paraformaldehyde (PFA) in 7.5% sucrose for 4 h. PFA was replaced with 15% sucrose (overnight–2 weeks). Hearts were dehydrated with increasing concentrations of ethanol (50%–100%) and xylene, then embedded in paraffin. Sections of 4 μm were prepared from the paraffin blocks.

The tissue sections were deparaffinized with xylene and rehydrated with alcohol (100%–50%), followed by standard HE staining. In addition, for dystrophin immunostaining, sections were rinsed in Triton X-100 for 10 min after rehydration. The sections were then placed in a 0.01 M citrate buffer solution, and pretreatment was performed in a microwave oven for 10 min. The sections were treated with a peroxidase block for 10 min, followed by a protein block for 60 min. The sections were incubated for 1 h with dystrophin antibody (Rabbit Polyclonal Antibody, Thermo Scientific, United States) at room temperature and washed with PBS for 5 min. Incubation of sections occurred with a biotin-labeled secondary antibody (Anti-Rabbit IgG Biotinylated Antibody, Vectastain Vector Laboratories) for 30 min, followed by washing in PBS for 5 min. Then, the sections were incubated with streptavidin peroxidase complex (ABC Kit, Vectastain, Vector Laboratories) for 30 min, followed by washing in PBS for 5 min. DAB chromogen (Liquid DAB Substrate Kit, Invitrogen) was added to all the sections for 2–3 min, followed by washing in water. Counterstaining was performed with Harris hematoxylin for 14 s. The sections were dehydrated in alcohol (50%–100%) and in xylene. The mounting was performed with a permount mounting medium. Images were taken using a light microscope (Olympus AX70).

2.5 | Data Analysis

Pixel-by-pixel analysis was performed to reconstruct the maps from the signal intensities using Aedes (http://aedes.uef.fi/) in MATLAB (Mathworks Inc., Natick, CA, United States). Regions of interest (ROIs) were manually drawn on the relaxation time maps in infarcted and remote myocardium to calculate the relative relaxation time difference (RRTD). RRTD was calculated to compare the relaxation times in two different ROIs in that relaxation time map. The infarct area was selected visually based on histology sections. The area opposite the infarct site, that is, the ventricular septum, was selected as a remote myocardium. RRTDs in LAD occluded mice were calculated as $(T\ (\text{infarct}) - T\ (\text{remote}))/T\ (\text{remote})$, where T is adiabatic $T_{1\rho}$, adiabatic $T_{2\rho}$, CW $T_{1\rho}$, T_2, or T_1 relaxation time averaged over infarct or remote area for both in vivo and ex vivo measurements. RRTDs in control mice in vivo were calculated as $(T\ (\text{whole myocardium}) - T\ (\text{chest muscles}))/T\ (\text{chest muscles})$. Results are given as the mean ± standard deviation. For the calculation of ejection fraction (EF), we defined end-systolic and end-diastolic volumes in the left ventricle. These volumes were drawn based on the endocardial border of the left ventricle in cine images. The statistical analysis was performed by one-way ANOVA, Student's *t*-test, and Bonferroni's multiple comparison. The data were assumed to follow a normal gaussian distribution, and the variances were homogenous. A corrected significance level of $p < 0.05$ was considered significant.

3 | Results

The MI was observed on the immobile area in cine images in vivo. The slice for relaxation time measurements was selected based on the largest cross section of the infarct in the cine images. The area of elevated relaxation time constants in both time points after the MI as compared to control mice in both adiabatic and CW $T_{1\rho}$ relaxation time maps and in $T_{2\rho}$ relaxation time maps was in the same area where the thinning of the myocardial wall in cine images in vivo was (Figure 2 and Figure S1). The adiabatic $T_{1\rho}$ relaxation times measured with both HS1 and HS4 pulses ($p<0.05$) and CW ($p<0.05$) were significantly elevated at the MI area already at the 2-h time point compared to controls (Table 1 and Figure 2). At Day 7 after MI, adiabatic $T_{1\rho}$ relaxation times with both HS1 and HS4 pulses ($p<0.05$) and CW ($p<0.05$) were clearly elevated at the MI area compared to controls (Table 1 and Figure 2). The RRTD values of $T_{1\rho}$ relaxation time constants with HS1, HS4, and CW pulses were elevated after the MI compared to controls ($p<0.05$) (Figure 3). The RRTD values of the adiabatic $T_{2\rho}$ relaxation times with the HS4 pulse were significantly elevated after the MI compared to controls ($p<0.05$) (Figure 3). In addition, there was a significant difference between RRTD values of $T_{2\rho}$ relaxation times with the HS1 and HS4 pulses in the 2-h time point ($p<0.01$) (Figure 3). A significant increase in T_2 relaxation time was found between controls and the 7-day time point MI area ($p<0.05$) (Table 1).

A clear difference in relaxation times between MI and remote myocardium was found visually with most of the relaxation times ex vivo. The relaxation time difference between MI and the remote area after 2 h of MI is visible with adiabatic $T_{1\rho}$ with both HS1 and HS4 pulses, and CW $T_{1\rho}$ and CW $T_{1\rho}$ showed the MI area the clearest (Figure 4). In addition, T_1 was increased in the same areas in the T_1 map as compared to all $T_{1\rho}$ maps (Figure 4). Additionally, the contrast is enhanced with adiabatic $T_{1\rho}$ with both HS1 and HS4 pulses and CW $T_{1\rho}$ from the 2-h to 7-day time point after MI (Figure 5). The visual interpretation is supported by the RRTD values, which were increased from the 2-h time point to the 7-day time point with adiabatic $T_{1\rho}$, with HS1 ($p<0.05$) and HS4 ($p<0.05$) pulses and CW $T_{1\rho}$ ($p<0.05$) (Figure 6). Adiabatic $T_{1\rho}$ with HS1 ($p<0.05$) and HS4 ($p<0.05$), CW $T_{1\rho}$ ($p<0.05$), and T_1 ($p<0.05$) relaxation time constants were significantly increased when comparing the intact hearts to the MI area

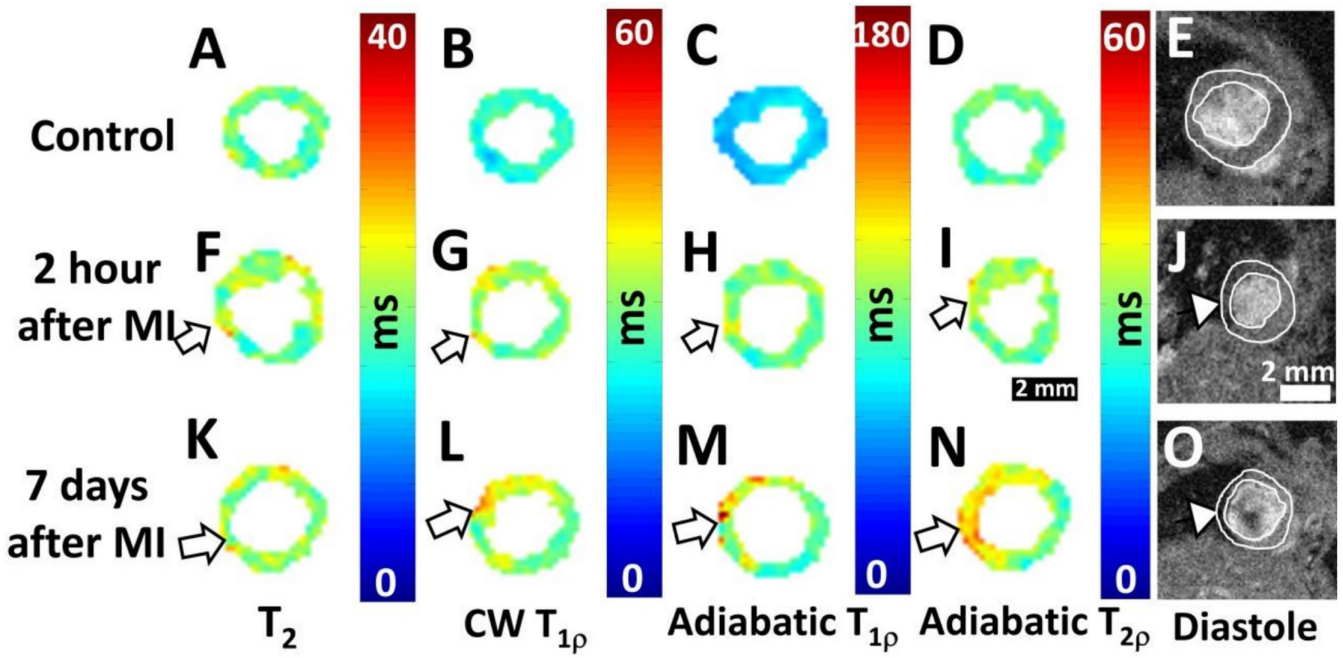

FIGURE 2 | In vivo relaxation time (T_2, CW $T_{1\rho}$, adiabatic $T_{1\rho}$ with HS4 pulse, and adiabatic $T_{2\rho}$ with HS4 pulse) maps and diastolic cine image (A–E) at the 2-h time point, respectively, and (F–J) at the 7-day time point after the MI. White arrows indicate the site of myocardial infarction.

TABLE 1 | Relaxation times from infarcted and remote areas of the MI group ($n=7$ in the 2-h time point and $n=5$ in the 7-day time point) and the control group ($n=4$) in vivo. The statistical analysis was performed by *t*-test and Bonferroni's multiple comparison correction between control and other areas (*$p<0.05$).

MRI sequence	Control (ms)	Infarct (ms) (MI after 2 h)	Remote (ms) (MI after 2 h)	Infarct (ms) (MI after 7 days)	Remote (ms) (MI after 7 days)
Adiab $T_{1\rho}$ HS4	62.5 ± 8.2	67.8 ± 12.5*	61.1 ± 10.9	81.7 ± 19.9*	67.0 ± 14.8
Adiab $T_{2\rho}$ HS4	36.7 ± 6.4	34.2 ± 3.9	29.3 ± 2.1	36.0 ± 1.0	30.0 ± 4.4
CW $T_{1\rho}$	26.9 ± 3.4	28.9 ± 3.0*	25.6 ± 1.7	34.0 ± 9.9*	27.5 ± 4.9
T_2	22.0 ± 2.0	21.8 ± 2.2	20.2 ± 3.0	23.7 ± 1.2*	21.7 ± 2.9

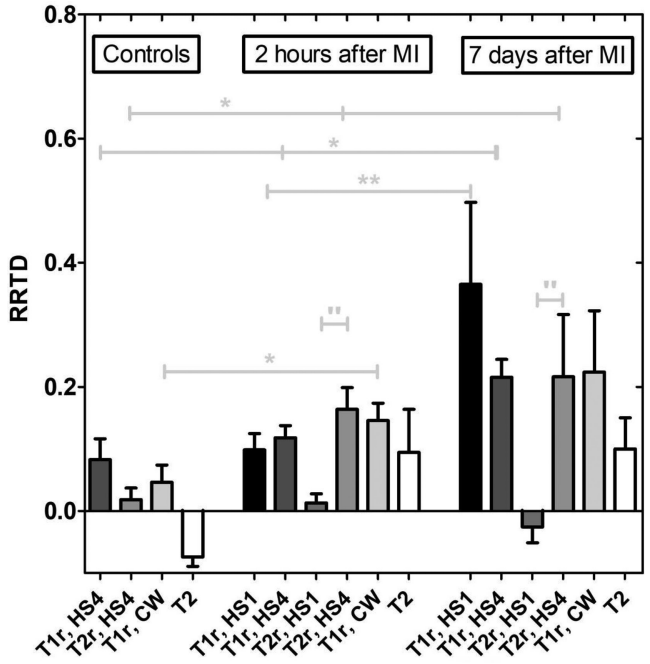

FIGURE 3 | In vivo RRTD values between MI and remote area at 2-h and 7-day time points and between similar areas in controls based on rotating frame relaxation times and T_2 in vivo (controls, $n=4$; the 2-h time point, $n=7$; and for the 7-day time point, $n=5$). The data is shown as mean ± standard deviation. (*$p<0.05$ and **$p<0.01$, one-way ANOVA, Bonferroni's multiple comparison correction for different time points, and "$p<0.01$, Students *t*-test for comparison with Bonferroni's correction to different methods).

of the 7-day time point (Table 2). In addition, CW $T_{1\rho}$ relaxation time constant was significantly increased already at the 2-h time point in the MI area as compared to intact hearts (Table 2). A significant RRTD increase was observed in adiabatic $T_{1\rho}$ with the HS1 pulse 7 days after MI compared to the acute time point ($p<0.05$) (Figure 6). The decrease of EF (controls: 58.3 ± 11.8%, MI after 2 h: 50.5 ± 13.3% and MI after 7 days: 47.9 ± 7.1%) was found after the MI as a function of time, which indicates that the function of the myocardium has decreased due to MI. The variation from the nominal value was found to be ± 11% for B_1 field homogeneity.

3.1 | Histological Verification

At the 2-h time point, HE staining was not able to visualize the MI area. Unlike HE staining, dystrophin immunohistostaining sensitively evaluates the immunohistochemical expression of dystrophin and shows the early stage of MI by the loss of sarcolemmal dystrophin staining and the focal loss of the fishnet pattern in the MI area [25]. In contrast to HE staining, the dystrophin immunohistostaining showed a clear MI area at both time points (Figure 7). Additionally, the damage caused by hypoxia in the myocardium was indicated by the partial loss of sarcolemmal dystrophin staining and focal loss of the fishnet patterns in the left ventricle at both time points (Figure 7). At the 7-day time point, the HE staining was able to reveal interstitial edema with increased eosinophilia of cardiac myocytes in the MI area (Figure 7). Differing from this, the dystrophin immunohistostaining showed a complete loss of sarcolemmal dystrophin staining, which indicates the fibrosis in the MI area (Figure 7).

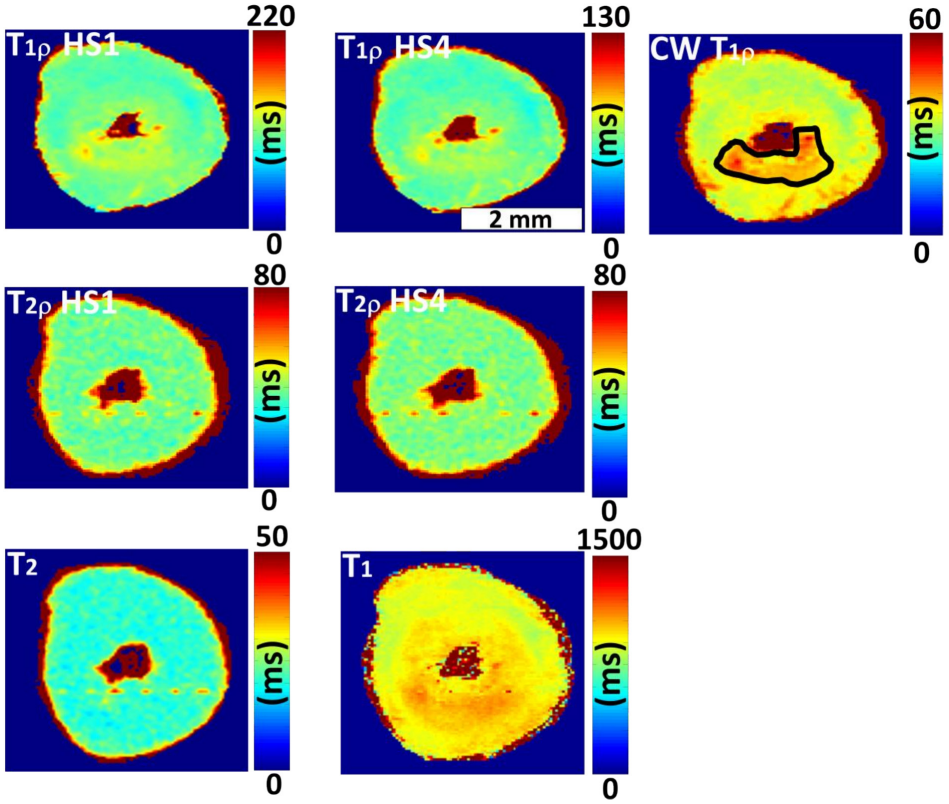

FIGURE 4 | Ex vivo relaxation time maps after 2 h of LAD occlusion with different rotating frames and conventional MRI methods. The outline of the selected ROI of infarct is presented with a black line in CW $T_{1\rho}$, and it was used in all relaxation time maps.

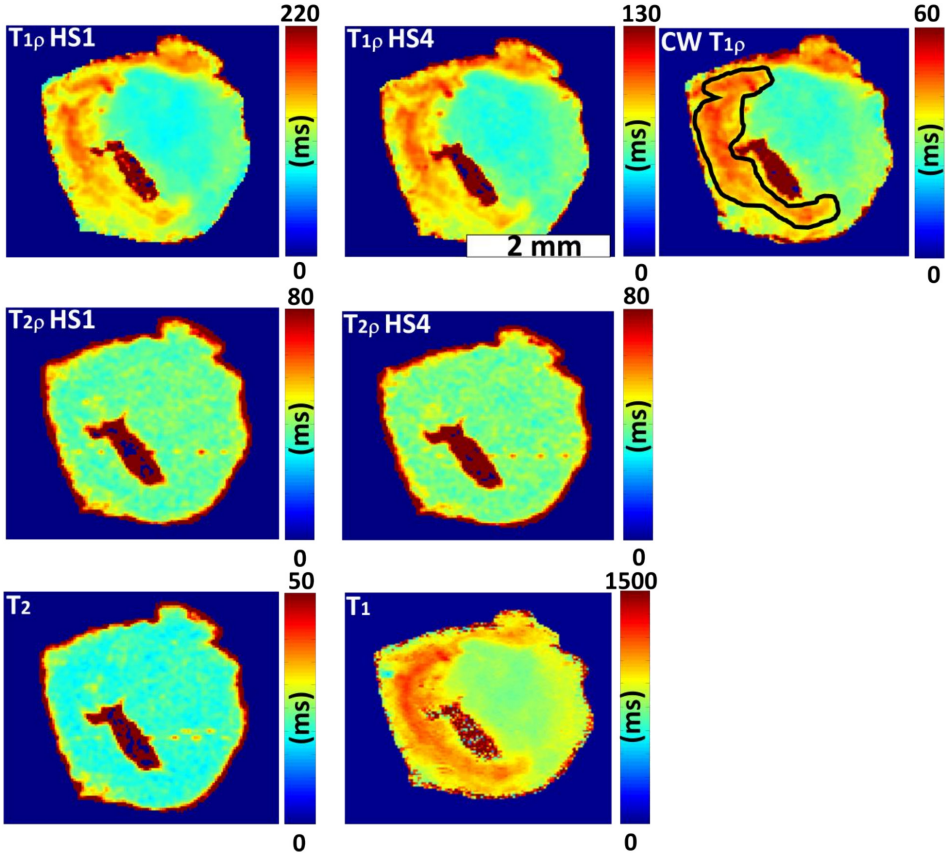

FIGURE 5 | Representative ex vivo relaxation maps after 7 days of LAD occlusion with different rotating frames and conventional MRI methods. The outline of the selected ROI of infarct is presented with a black line in CW $T_{1\rho}$, and it was used in all relaxation time maps.

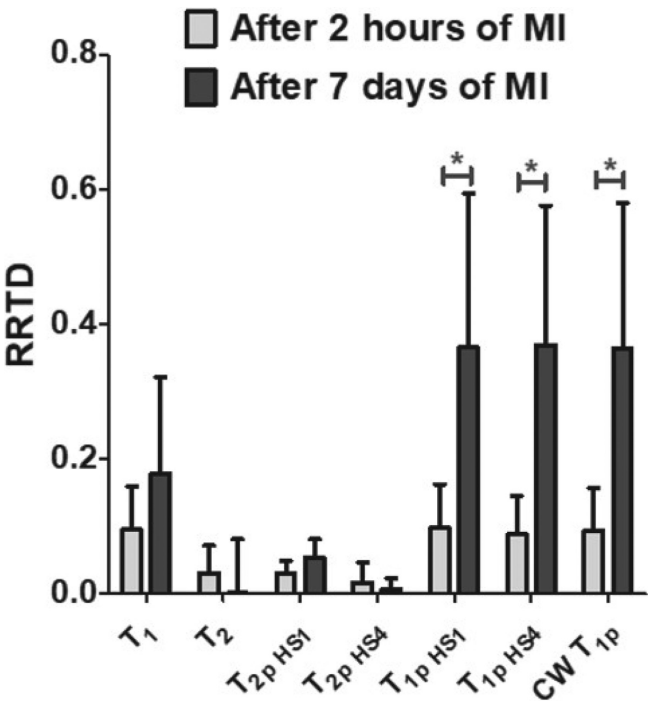

FIGURE 6 | Ex vivo RRTD values (mean ± SD). The values are calculated from T_1, T_2, $T_{1\rho}$, $T_{1\rho\,HS1}$, $T_{1\rho\,HS4}$, $T_{2\rho\,HS1}$, and $T_{2\rho\,HS4}$ relaxation time maps ex vivo ($n = 10$). The data is shown as mean ± standard deviation. (*$p < 0.05$, Student's *t*-test with Bonferroni's correction).

By a visual comparison between the different relaxation time maps and both histological stainings, our findings indicated that the increased relaxation time constants in the relaxation time maps were seen in the same areas as the damaged tissue in histologically stained sections.

4 | Discussion

Rotating frame relaxation time constants were characterized in the mouse heart in and ex vivo after 2 h and 7 days of MI. Adiabatic $T_{1\rho}$ with both HS1 and HS4 pulses and adiabatic $T_{2\rho}$ with HS4 showed high contrast differences between the MI and remote areas after 2 h and 7 days of MI in vivo. Ex vivo measurements of adiabatic $T_{1\rho}$ with both HS1 and HS4 pulses, CW $T_{1\rho}$ and T_1 showed higher RRTDs compared to T_2 and adiabatic $T_{2\rho}$ measurements.

The contrast difference between MI and remote areas was already increased 2 h after the MI with adiabatic $T_{1\rho}$ with both HS1 and HS4 pulses and CW $T_{1\rho}$ and continued to increase 7 days after MI in vivo. The increase was expected since $T_{1\rho}$ relaxation time is known to be sensitive to the formation of granulation tissue, which has been previously found in mouse MI studies [9, 13, 14, 26]; however, the increase of $T_{1\rho}$ relaxation time constant in the 2-h time point might be caused by other biological phenomena such as inflammation. Seven days after MI was considered a subchronic phase of MI, the time point is

TABLE 2 | MR relaxation times from infarcted areas, remote areas ($n=5$ in the 2-h time point and $n=5$ in the 7-day time point), and control hearts ($n=4$) ex vivo. The statistical analysis was performed by *t*-test and Bonferroni's multiple comparison correction between control and other areas (*$p<0.05$).

MRI sequence	Controls (ms)	Infarct (ms) (MI after 2 h)	Remote (ms) (MI after 2 h)	Infarct (ms) (MI after 7 days)	Remote (ms) (MI after 7 days)
Adiab $T_{1\rho}$ HS1	74.5 ± 0.3	93.8 ± 21.8	85.5 ± 20.0	127.7 ± 37.1*	92.3 ± 16.0*
Adiab $T_{1\rho}$ HS4	47.8 ± 1.3	58.3 ± 12.3	53.5 ± 10.3	78.3 ± 20.4*	56.7 ± 9.0
Adiab $T_{2\rho}$ HS1	40.0 ± 3.6	39.8 ± 2.0	38.7 ± 1.5	38.0 ± 1.4	37.0 ± 0.0
Adiab $T_{2\rho}$ HS4	40.5 ± 1.2	40.5 ± 10.5	39.8 ± 11.7	39.7 ± 1.2	39.3 ± 0.6
CW $T_{1\rho}$	21.8 ± 1.3	27.5 ± 6.8*	25.0 ± 5.3	37.7 ± 10.2*	27.3 ± 4.5*
T_2	22.7 ± 0.5	22.0 ± 0.6	21.7 ± 1.0	21.3 ± 1.5	21.3 ± 1.2
T_1	463.3 ± 26.1	562.7 ± 107.3	517.0 ± 118.5	691.5 ± 165.9*	587.0 ± 125.5

still fairly early for scar tissue formation, and it is highly warranted to determine the biomarkers in the subchronic phase of MI. It has been shown that MI consists of 90% necrotic tissue after 2 days of MI, transforming into granulation tissue and finally into scar tissue after 14 days of permanent occlusion in a mouse model [27]. At this point, when the presence of scar tissue is more sufficient, the $T_{1\rho}$ relaxation time constant has been found to be elevated [9, 13, 14, 26]. Additionally, $T_{1\rho}$ relaxation is selectively sensitive to low-frequency macromolecular interactions and slow molecular motions (long correlation times), while conventional T_1 relaxation is selectively sensitive to Larmor frequency and T_2 is nonselective for low-frequency motions [28]. These differences may explain the higher RRTD values in both adiabatic and CW $T_{1\rho}$ relaxation time maps compared to T_1 and T_2. The significant increase in $T_{1\rho}$ after 7 days compared to the nonsignificant increase after 3 days of LAD occlusion [13] indicated that the increased $T_{1\rho}$ relaxation time constant might first react to the edema and inflammation, but it reacts more at later MI development phases after the acute phase of MI since $T_{1\rho}$ is speculated to be affected by collagen, the interstitial water content, and the exchange of protons between hydroxyl and amide groups [9, 13, 14, 27, 28]. One major limitation of both $T_{1\rho}$ and $T_{2\rho}$ relaxation time measurements is the high specific absorption rate (SAR). The CW $T_{1\rho}$ technique is the classical way to acquire the rotating frame method; however, adiabatic techniques have been developed to be more tolerant to frequency artifacts, making it a more robust technique compared to CW [29]. This is important to know when these techniques are translated into a clinical setting.

Interestingly, the RRTD of adiabatic $T_{2\rho}$ with HS4 pulse is increasing as a function of time after MI and has the highest RRTD value 7 days after the MI. This might be explained by the sensitivity to the increased amount of free water caused by edema and the formation of granulation tissue. The differences in relaxation mechanisms behind the $T_{1\rho}$ and $T_{2\rho}$ relaxation times may explain slight differences between hyperintensity areas of $T_{1\rho}$ and $T_{2\rho}$ relaxation time maps. Additionally, T_2 increased in the same areas as in $T_{2\rho}$, supporting our results. In addition, there is a significant difference in $T_{2\rho}$ RRTD values between HS1 and HS4 pulses at the 2-h time point indicating $T_{2\rho}$ with HS4 pulse is able to create more contrast between MI and remote areas in both time points compared to $T_{2\rho}$ with HS1 pulse. Furthermore, MI was barely visible in $T_{2\rho}$ relaxation time mapping with either pulse ex vivo. This might be explained by the differences in blood contribution and the increased amount of free water in the living myocardium, with other physiological differences in the myocardium after the MI. Additionally, tissue fixation decreases the relaxation times ex vivo compared to in vivo. The difference between HS1 and HS4 can be explained by the difference in stretching factors affecting amplitude and frequency modulation functions, M trajectories, and the signal decay during the pulse train. $T_{1\rho}$ measured with both HS1 and HS4 increases simultaneously but less intensively than adiabatic $T_{2\rho}$ with HS4.

Ex vivo measurements of CW $T_{1\rho}$ and adiabatic $T_{1\rho}$ with both HS1 and HS4 pulse wave forms showed the highest RRTDs, with a significant RRTD increase from the 2-h time point to 7 days after the MI. Significant increases in relaxation time constants support the findings of the in vivo measurements. The findings of in vivo and ex vivo adiabatic $T_{1\rho}$ relaxation time constants are like previous CW $T_{1\rho}$ findings [9, 13, 14, 21], indicating that $T_{1\rho}$ is more sensitive to scar formation than to the acute edema reaction, whereas our finding of elevated adiabatic $T_{2\rho}$ with HS4 pulse in the acute phase indicates $T_{2\rho}$ sensitivity to acute biological tissue changes after MI.

Previous studies showed a shorter T_1 relaxation time ex vivo than in vivo at 9.4 T [30, 31]. T_1 relaxation is related to protein–water interactions, and tissue fixation leads to protein crosslinking that reduces tissue T_1 relaxation time [32]. The T_1 relaxation time is increasing in the area of MI, suggesting that the area of MI consists of protein–water interactions. However, several factors can affect the T_1 relaxation time, including the fridge and room temperature, the concentration of fixative PFA, the storage solution of 15% sucrose, and magnetic field strength [33–35]. Additionally, ex vivo measurements are affected by the lack of free water in the myocardium after fixation of the hearts using PFA; there are different spin dynamics and relaxation mechanisms as compared to in vivo measurements. These factors may also affect the rotating frame relaxation times ex vivo. However, these variables were kept as constant as possible for all the ex vivo measurements of this study.

MI areas were verified with two histological stainings: HE and dystrophin immunostaining. The HE staining was initially performed to verify MI at both time points (2 h and 7 days after MI);

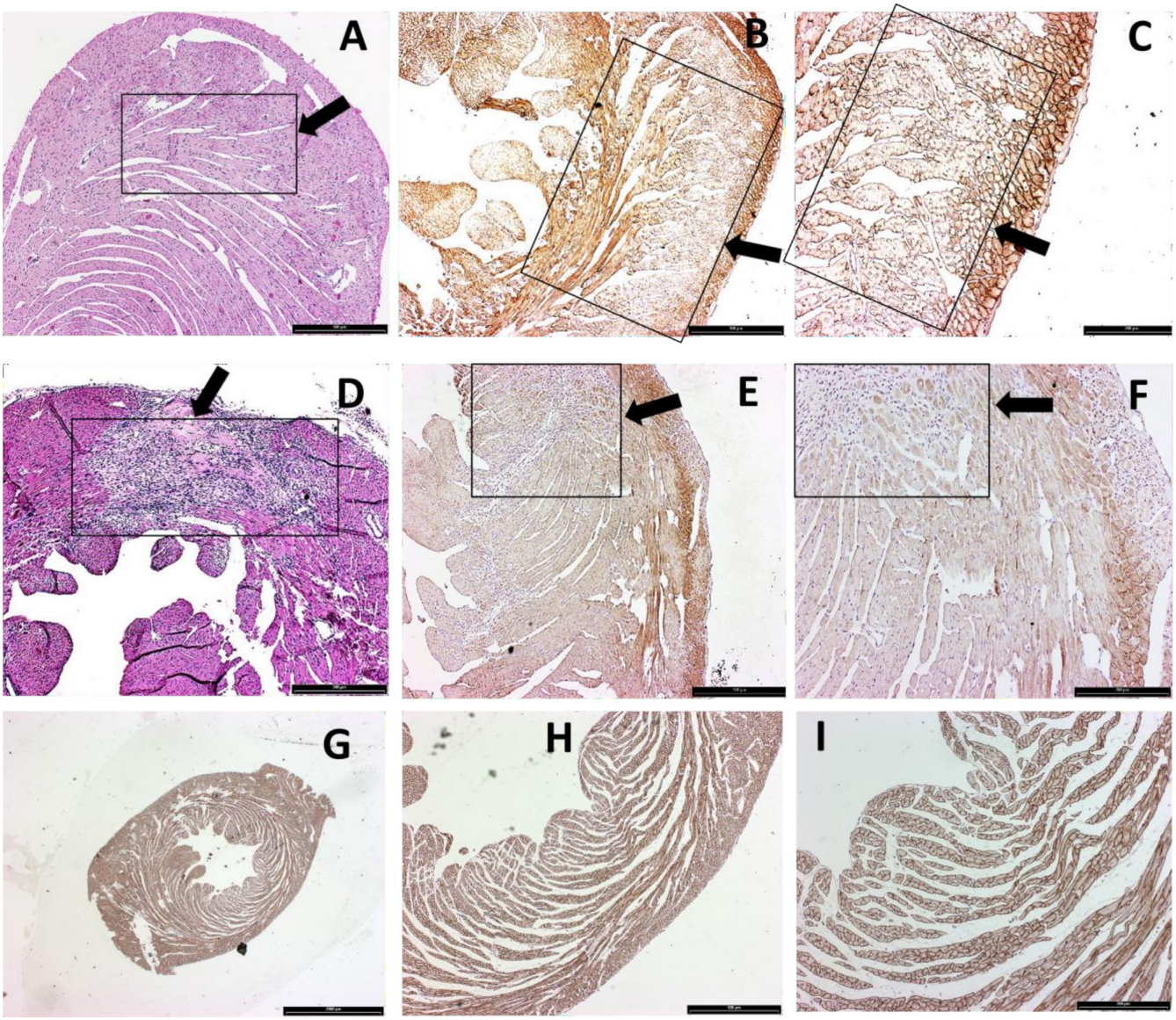

FIGURE 7 | Histology images of myocardium at both time points taken by light microscope (A) hematoxylin–eosin stain after 2 h (4× magnification), (B) dystrophin immunostaining after 2 h (4× magnification), (C) dystrophin immunostaining after 2 h (10× magnification), (D) hematoxylin–eosin stain after 7 days (4× magnification), (E) dystrophin immunostaining after 7 days (4× magnification), and (F) dystrophin immunostaining after 7 days (10× magnification), where the black arrow is pointing to the infarction area. Histology images (G–I) are from an intact heart with dystrophin immunostaining, so that G is 1.25× magnification, H is 4× magnification, and I is 10× magnification. The heart in A–C is the same heart as in Figure 4, and the heart in D–F is the same heart as in Figure 5.

however, it showed differences between MI and remote tissues only after 7 days of MI. HE staining was found to be inefficient for differentiating MI and remote myocardium 2 h after LAD occlusion. In acute myocardial ischemia, where acute edema reaction is dominant, the reaction is characterized by the swelling of cells and damage to the sarcolemma and membrane-associated proteins; however, to our knowledge, HE is not a specific histological method to determine acute edema reaction. Dystrophin immunohistochemical staining showed clear differences between the remote and MI tissue after 2 h and after 7 days of infarction. This finding is relevant since dystrophin is an efficient staining method for differentiating the MI area from remote tissue at the early stages of infarction due to the loss of sarcolemmal dystrophin staining in infarcted areas [36–39]. Cardiomyocytes contain a group of proteins called dystrophin-associated proteins, which, with dystrophin, form a complex that is involved in stabilizing the plasma membrane [38]. Additionally, dystrophins link the laminin receptor and dystrophin complex to the intracellular cytoskeletal talin and actin, and in the case of MI, subsarcolemma bleb formation is followed by the loss of dystrophin from the membrane [37]. Importantly, visually dystrophin staining highlighted the same areas in the myocardium as the increased relaxation time constants in the maps. However, the exact matching and comparison of a 4 μm histological section to a 1 mm thick MRI slice is difficult, and to our knowledge, there is no perfect method to do the comparison between the diastolic phase of cardiac MRI and histological sections from unknown cardiac cycles. Thus, this limitation needs to be considered when comparing the cardiac MRI and histological sections and making the conclusion based on the results.

This preclinical mouse study had some limitations. First, the number of mice could be larger to gain more statistical power for both in vivo and ex vivo measurements. Additionally, a possible partial volume effect artifact in the heart–lung interface might have affected the results. Also, motion artifacts due to failure or partial failure of the ECG and respiratory triggering might have caused some deviation from the results by affecting the quality of the weighted images. Secondly, due to timing difficulties and the tail vein injections, it was not possible to include a comparative LGE imaging in the imaging protocol, and thus, we cannot compare our results to the LGE method. Additionally, our in vivo T_1 and HS1 pulse measurements were not measured due to technical difficulties and too long anesthesia time for mice. Thirdly, the exact matching between the histological sections and relaxation time constant maps is challenging; however, the visual correlation by localizing the right ventricular and papillary muscles between MRI and histology was done to give qualitative verification. To point out, in vivo images were acquired during the diastole phase of the heart cycle and ex vivo images were acquired from the same phase as the histology sections. Fourthly, the 7-day time point after MI has been used as a subchronic phase of mouse MI; however, that time period might not be enough for the formation of scar tissue, and therefore, a later time point after the MI is needed for detecting the actual scar formation. In addition, there has been biological variability in mice and the success of the MI operation, which might have affected the results of this manuscript. Thus, the study would benefit from sham-operated mice to find the effect of surgical operation on the relaxation times. Despite these limitations of the study, all the results are promising. Rotating frame relaxation time methods can determine MI area in the acute and chronic phases of MI with $T_{1\rho}$ and $T_{2\rho}$ relaxation time methods in and ex vivo mouse models, which indicates the potential of these endogenous contrasts for infarct visualization without contrast agents.

As a conclusion, this MI study of mouse hearts shows that both adiabatic and CW $T_{1\rho}$ relaxation methods provide possibilities for follow-up studies of MI and might provide potential noninvasive diagnostic markers for tissue damage after MI. Additionally, adiabatic $T_{2\rho}$ with HS4 pulse relaxation time mapping determines both acute and subchronic MI after 7 days of LAD occlusion. In addition, dystrophin-based immunohistochemical staining showed clear differences between acute infarct and normal tissue, supporting the results of relaxation time maps.

Author Contributions

E.Y.-H., H.L., and M.A.K. did programming and magnetic resonance imaging, analyzed the data, and wrote the manuscript. S.L. and T.H. contributed to surgery, histology, and tissue processing. T.L. and S.Y.-H. contributed to the design, data analysis, writing, and editing of the manuscript. All the authors have read and approved the manuscript.

Acknowledgments

The authors thank the laboratory and MR maintenance staff members Maarit Pulkkinen and Jari Nissinen for their help and support during the measurements. Open access publishing facilitated by Ita-Suomen yliopisto, as part of the Wiley - FinELib agreement.

Disclosure

This work/part of the work was carried out with the support of Kuopio Biomedical Imaging Unit, University of Eastern Finland, Kuopio, Finland (part of Biocenter Kuopio, Finnish Biomedical Imaging Node, and EuroBioImaging).

Ethics Statement

All animal experiments were performed according to the national and international guidelines for laboratory animal use and under license ESAVI-270-04.10.07-2017 approved by the National Animal Experiment Board of Finland. All procedures performed in this study were in accordance with the ethical standards of the National Animal Experiment Board in Finland (Eläinkoelautakunta, ELLA).

Conflicts of Interest

The authors declare no conflicts of interest.

References

1. S. S. Virani, A. Alonso, H. J. Aparicio, et al., "Heart Disease and Stroke Statistics-2021 Update: A Report From the American Heart Association," *Circulation* 143, no. 8 (2021): e254–e743, https://doi.org/10.1161/CIR.0000000000000950.

2. K. Thygesen, J. S. Alpert, A. S. Jaffe, et al., "Third Universal Definition of Myocardial Infarction," *European Heart Journal* 33, no. 20 (2012): 2551–2567.

3. E. Falk, P. K. Shah, and V. Fuster, "Coronary Plaque Disruption," *Circulation* 92, no. 3 (1995): 657–671, https://doi.org/10.1161/01.CIR.92.3.657.

4. P. S. Rajiah, C. J. François, and T. Leiner, "Cardaic MRI: State of the Art," *Radiology* 307, no. 3 (2023): e223008.

5. C. Klein, T. R. Schmal, S. G. Nekolla, B. Schnackenburg, E. Fleck, and E. Nagel, "Mechanism of Late Gadolinium Enhancement in Patients With Acute Myocardial Infarction," *Journal of Cardiovascular Magnetic Resonance* 9, no. 4 (2007): 653–658, https://doi.org/10.1080/10976640601105614.

6. E. Ylä-Herttuala, A. Saraste, J. Knuuti, T. Liimatainen, and S. Ylä-Herttuala, "Molecular Imaging to Monitor Left Ventricular Remodeling in Heart Failure," *Current Cardiovascular Imaging Reports* 12 (2019): 11, https://doi.org/10.1007/s12410-019-9487-3.

7. Y. Amano, M. Tachi, H. Tani, K. Mizuno, Y. Kobayashi, and S. Kumita, "T_2-Weighted Cardiac Magnetic Resonance Imaging of Edema in Myocardial Diseases," *ScientificWorldJournal* 2012 (2012): 194069, https://doi.org/10.1100/2012/194069.

8. R. J. Beyers, R. S. Smith, Y. Xu, et al., "T_2-Weighted MRI of Post-Infarct Myocardial Edema in Mice," *Magnetic Resonance in Medicine* 67, no. 1 (2012): 201–209, https://doi.org/10.1002/mrm.22975.

9. E. Yla-Herttuala, S. Laidinen, H. Laakso, and T. Liimatainen, "Quantification of Myocardial Infarct Area Based on T_{RAFFn} Relaxation Time Maps - Comparison With Cardiovascular Magnetic Resonance Late Gadolinium Enhancement, $T_{1\rho}$ and T_2 In Vivo," *Journal of Cardiovascular Magnetic Resonance* 20 (2018): 34, https://doi.org/10.1186/s12968-018-0463-x.

10. W. R. Witschey, J. J. Pilla, G. Ferrari, et al., "Rotating Frame Spin Lattice Relaxation in a Swine Model of Chronic, Left Ventricular Myocardial Infarction," *Magnetic Resonance in Medicine* 64, no. 5 (2010): 1453–1460, https://doi.org/10.1002/mrm.22543.

11. S. Berisha, J. Han, M. Shahid, Y. Han, and W. R. T. Witschey, "Measurement of Myocardial $T_{1\rho}$ With a Motion Corrected, Parametric Mapping Sequence in Humans," *PLoS ONE* 11, no. 3 (2016): e0151144, https://doi.org/10.1371/journal.pone.0151144.

12. M. I. Kettunen, O. H. Gröhn, M. Penttonen, and R. A. Kauppinen, "Cerebral $T_{1\rho}$ Relaxation Time Increases Immediately Upon Global Ischemia in the Rat Independently of Blood Glucose and Anoxic Depolarization," *Magnetic Resonance in Medicine* 46 (2001): 565–572, https://doi.org/10.1002/mrm.1228.

13. H. S. Musthafa, G. Dragneva, L. Lottonen, et al., "Longitudinal Rotating Frame Relaxation Time Measurements in Infarcted Mouse Myocardium In Vivo," *Magnetic Resonance in Medicine* 69, no. 5 (2013): 1389–1395, https://doi.org/10.1002/mrm.24382.

14. E. Ylä-Herttuala, T. Vuorio, S. Kettunen, S. Laidinen, S. Ylä-Herttuala, and T. Liimatainen, "Lymphatic Insufficiency Leads to Distinct Myocardial Infarct Content Assessed by Magnetic Resonance T_{RAFFn}, $T_{1\rho}$ and T_2 Relaxation Times," *Scientific Reports* 13 (2023): 1579, https://doi.org/10.1038/s41598-023-28219-6.

15. J. W. van Oorschot, F. Guclu, S. de Jong, et al., "Endogenous Assessment of Diffuse Myocardial Fibrosis in Patients With T1ρ- Mapping," *Journal of Magnetic Resonance Imaging* 45, no. 1 (2017): 132–138.

16. S. Michaeli, D. J. Sorce, C. S. Springer, Jr., K. Ugurbil, and M. Garwood, "T1rho MRI Contrast in the Human Brain: Modulation of the Longitudinal Rotating Frame Relaxation Shutter-Speed During an Adiabatic RF Pulse," *Journal of Magnetic Resonance* 181, no. 1 (2006): 135–147, https://doi.org/10.1016/j.jmr.2006.04.002.

17. S. Michaeli, D. J. Source, D. Idiyatullin, K. Ugurbil, and M. Garwood, "Transverse Relaxation in the Rotating Frame Induced by Chemical Exchange," *Journal of Magnetic Resonance* 169, no. 2 (2004): 293–299.

18. M. Garwood and L. DelaBarre, "The Return of the Frequency Sweep: Designing Adiabatic Pulses for Contemporary NMR," *Journal of Magnetic Resonance* 153, no. 2 (2001): 155–177.

19. J. Ellermann, W. Ling, M. J. Nissi, et al., "MRI Rotating Frame Relaxation Measurements for Articular Cartilage Assessment," *Magnetic Resonance Imaging* 31, no. 9 (2013): 1537–1543, https://doi.org/10.1016/j.mri.2013.06.004.

20. S. Michaeli, H. Gröhn, O. Gröhn, et al., "Exchange-Influenced T2rho Contrast in Human Brain Images Measured With Adiabatic Radio Frequency Pulses," *Magnetic Resonance in Medicine* 53, no. 4 (2005): 823–829, https://doi.org/10.1002/mrm.20428.

21. A. Bustin, S. Toupin, S. Sridi, et al., "Endogenous Assessment of Myocardial Injury With Single-Shot Model-Based Non-Rigid Motion-Corrected T1 Rho Mapping," *Journal of Cardiovascular Magnetic Resonance* 23 (2021): 119, https://doi.org/10.1186/s12968-021-00781-w.

22. I. Räty, A. Aarnio, and M. J. Nissi, "*Ex Vivo* Imaging of Subacute Myocardial Infarction With Ultra-Short Echo Time 3D Quantitative T_1- and $T_1\rho$-Mapping Magnetic Resonance Imaging in Mice," *European Heart Journal - Imaging Methods and Practice* 3, no. 1 (2025): qyae131, https://doi.org/10.1093/ehjimp/qyae131.

23. C. Coletti, A. Fotaki, J. Tourais, et al., "Robust Cardiac T1ρ Mapping at 3T Using Adiabatic Spin-Lock Preparations," *Magnetic Resonance in Medicine* 90, no. 4 (2023): 1363–1379, https://doi.org/10.1002/mrm.29713.

24. O. H. J. Gröhn, M. I. Kettunen, H. I. Mäkelä, et al., "Early Detection of Irreversible Cerebral Ischemia in the Rat Using Dispersion of the Magnetic Resonance Imaging Relaxation Time, T1rho," *Journal of Cerebral Blood Flow and Metabolism* 20, no. 10 (2000): 1457–1466, https://doi.org/10.1097/00004647-200010000-00007.

25. H. Thomsen and H. Held, "Immunohistochemical Detection of C5b-9 (m) in Myocardium: An Aid in Distinguishing Infarction-Induced Ischemic Heart Muscle Necrosis From Other Forms of Lethal Myocardial Injury," *Forensic Science International* 71, no. 2 (1995): 87–95, https://doi.org/10.1016/0379-0738(94)01640-Q.

26. W. R. T. Witschey, G. A. Zsido, and K. Koomalsingh, "In Vivo Chronic Myocardial Infarction Characterization by Spin Locked Cardiovascular Magnetic Resonance," *Journal of Cardiovascular Magnetic Resonance* 14 (2012): 37, https://doi.org/10.1186/1532-429X-14-37.

27. J. I. Virag and C. E. Murry, "Myofibroblast and Endothelial Cell Proliferation During Murine Myocardial Infarct Repair," *American Journal of Pathology* 163, no. 6 (2003): 2433–2440, https://doi.org/10.1016/S0002-9440(10)63598-5.

28. S. Michaeli, T. C. Burns, E. Kudishevich, et al., "Detection of Neuronal Loss Using T(1rho) MRI Assessment of (1)H(2)O Spin Dynamics in the Aphakia Mouse," *Journal of Neuroscience Methods* 177, no. 1 (2009): 160–167, https://doi.org/10.1016/j.jneumeth.2008.10.025.

29. T. Vuorio, E. Ylä-Herttuala, J. P. Laakkonen, S. Laidinen, T. Liimatainen, and S. Ylä-Herttuala, "Downregulation of VEGFR3 Signaling Alters Cardiac Lymphatic Vessel Organization and Leads to a Higher Mortality After Acute Myocardial Infarction," *Scientific Reports* 8 (2018): 16709, https://doi.org/10.1038/s41598-018-34770-4.

30. L. Wu, C. Carchi, S. Michaeli, S. Mangia, and D. Idiyatullin, "Alternating Look-Locker for Quantitative T_1, $T_{1\rho}$ and B_1 3D MRI Mapping," *Magnetic Resonance in Medicine* 91 (2024): 149–161, https://doi.org/10.1002/mrm.29839.

31. V. Casula, J. Karjalainen, V. Mlynarik, et al., "Does T1ρ Measure Proteoglycan Concentration in Cartilage?," *Journal of Magnetic Resonance Imaging* 59 (2024): 1874–1875, https://doi.org/10.1002/jmri.28981.

32. A. J. Bakermans, D. Abdurrachim, T. R. Geraedts, S. M. Houten, K. Nicolay, and J. J. Prompers, "In Vivo Proton T1 Relaxation Times of Mouse Myocardial Metabolites at 9.4 T," *Magnetic Resonance in Medicine* 73, no. 6 (2015): 2069–2074, https://doi.org/10.1002/mrm.25340.

33. W. Li, M. Griswold, and X. Yu, "Rapid T1 Mapping of Mouse Myocardium With Saturation Recovery Look-Locker Method," *Magnetic Resonance in Medicine* 64, no. 5 (2010): 1296–1303, https://doi.org/10.1002/mrm.22544.

34. M. R. Raman, Y. Shu, T. G. Lesnick, C. R. Jack, and K. Kantarci, "Regional T1 Relaxation Time Constants in Ex Vivo Human Brain: Longitudinal Effects of Formalin Exposure," *Magnetic Resonance in Medicine* 77, no. 2 (2017): 774–778, https://doi.org/10.1002/mrm.26140.

35. J. P. Korb and R. G. Bryant, "Magnetic Field Dependence of Proton Spin-Lattice Relaxation Times," *Magnetic Resonance in Medicine* 48, no. 1 (2002): 21–26, https://doi.org/10.1002/mrm.10185.

36. W. D. Rooney, G. Johnson, X. Li, et al., "Magnetic Field and Tissue Dependencies of Human Brain Longitudinal 1H2O Relaxation in Vivo," *Magnetic Resonance in Medicine* 57, no. 2 (2007): 308–318, https://doi.org/10.1002/mrm.21122.

37. P. A. Rinck, H. W. Fischer, L. Vander Elst, Y. Van Haverbeke, and R. N. Muller, "Field-Cycling Relaxometry: Medical Applications," *Radiology* 168, no. 3 (1988): 843–849, https://doi.org/10.1148/radiology.168.3.3406414.

38. J. Ouyang, M. Guzman, F. Desoto-Lapaix, M. R. Pincus, and R. Wieczorek, "Utility of Desmin and a Masson's Trichrome Method to Detect Early Acute Myocardial Infarction in Autopsy Tissues," *International Journal of Clinical and Experimental Pathology* 3, no. 1 (2009): 98–105.

39. S. Hashmi and S. Al-Salam, "Loss of Dystrophin Staining in Cardiomyocytes: A Novel Method for Detection Early Myocardial Infarction," *International Journal of Clinical and Experimental Pathology* 6, no. 2 (2013): 249–257.

Supporting Information

Additional supporting information can be found online in the Supporting Information section.